Cellulose
https://doi.org/10.1007/s10570-025-06860-w

ORIGINAL RESEARCH

Role of composition and molecular weight on the dissolution of cellulosic yarns

Nora S. Alrefaei · Peter J. Hine · Michael E. Ries

Received: 27 February 2025 / Accepted: 13 November 2025

Abstract In this work we show that it is the molecular weight in a variety of natural and treated plant yarns that is the dominant factor in controlling both the rate of dissolution and the dissolution activation energy in the ionic liquid 1-ethyl-3-methylimidazolium acetate. We have used an alkali treatment (sodium hydroxide) to primarily reduce the molecular weight of three natural plant yarns (hemp, cotton and flax) in order to investigate how dissolution depends on molecular weight, composition and crystallinity. Dissolution experiments were carried out on both the raw and alkali-treated yarns. Chemical composition, crystallinity, and molecular weight were determined for all these six yarns. After dissolution, the partially dissolved yarns were coagulated in water, resulting in a composite material with an undissolved inner core surrounded by a dissolved and coagulated outer skin region. The growth of this dissolved and coagulated fraction was tracked using optical microscopy, showing it to increase with dissolution time and temperature. Time–temperature superposition was found to hold in all cases, allowing a dissolution activation energy to be determined. The width of the outer skin of the coagulated region was found to be directly proportional to the square root of the dissolution time, demonstrating that the limiting factor for dissolution is the diffusion of the ionic liquid. Finally, all the mercerised yarns were found to dissolve faster than their natural versions, suggesting that molecular weight is a contributing factor in affecting the speed of dissolution.

Keywords Cellulose · Ionic liquid · Molecular weight · Composition · Dissolution · Activation energy

Introduction

Natural cellulose-based yarns are attracting increased attention as promising raw materials, notably in areas such as construction materials and automotive vehicles (Crini et al. 2020). These yarns are highly valued as renewable and eco-friendly alternatives to synthetic fibres, and furthermore, their recyclability and lightweight properties align with the industrial aims to minimize product weight, enhancing their appeal in various sectors (Brodin et al. 2017). Cellulosic yarns primarily consist of cellulose, hemicellulose, and lignin as their fundamental components, often accompanied by pectin

Supplementary Information The online version contains supplementary material available at https://doi.org/10.1007/s10570-025-06860-w.

N. S. Alrefaei
Department of Physics, Faculty of Science, Taibah University, Yanbu, Saudi Arabia

N. S. Alrefaei · P. J. Hine · M. E. Ries (✉)
School of Physics and Astronomy, University of Leeds, Woodhouse Lane, Leeds LS2 9JT, UK
e-mail: m.e.ries@leeds.ac.uk

Published online: 23 November 2025

and wax substances (Okolie et al. 2021; Hasan et al. 2022). Hemp, cotton, and flax boast substantial cellulose content of 74%, 92%, and 81%, respectively (Mwaikambo and Ansell 2002).

Natural yarns exhibit a propensity for moisture absorption, and when combined with a hydrophobic matrix, this results in yarn swelling within the composite structure (Moudood et al. 2019; Mohammed et al. 2023). This can compromise the interfacial bond, leading to complexities such as dimensional instability, matrix fracturing, and a consequent decline in the comprehensive mechanical properties of the composites (Sethi and Ray 2015). Additionally, the abundance of surface impurities and the significant presence of hydroxy groups in plant yarns render them a less appealing choice for strengthening polymeric materials (Mwaikambo and Ansell 2002). To address this concern, enhancing yarn surface roughness through appropriate treatments is crucial to the composite fabrication process (Balaji and Nagarajan 2017). The adoption of a sodium hydroxide (NaOH) treatment, often termed alkali treatment, has garnered widespread acceptance as a chemical pretreatment for cellulosic yarns (Ying Wang 2008; Kalia et al. 2011). Studies reported that this alteration enhances the yarns' resistance to moisture by reducing the presence of hydrophilic hydroxy groups. Furthermore, alkali treatment induces significant changes by increasing surface roughness, disrupting hydrogen bonding within the network structure, which ultimately contributes to improving the composite's mechanical properties (Modibbo et al. 2009; Mbada et al. 2016; Ahmad et al. 2019). Prior investigations, such as MacDonald et al.'s study in 1983, examined the effects of NaOH pre-treatment on corn stover under various conditions. The results indicated partial solubilisation of lignin and hemicellulose fractions, influenced by factors such as NaOH concentration, temperature, and reaction time, while the cellulose component remained relatively unaffected. Similarly, Xu et al. (2010) explored the impact of NaOH pre-treatment on switchgrass, an herbaceous feedstock, reporting partial solubilisation of lignin and hemicellulose. The NaOH pre-treatment of natural yarns, as elucidated by Boey et al. (2022), demonstrated it effectively removes lignin, pectin, waxy materials, and natural oils that typically coat the outer surface of the yarn cell wall. This process exposes the fibrils and imparts a rough surface texture to the yarn (Patil et al. 2019). The interaction of NaOH with cellulose, known as alkalization, is described in Eq. 1

$$\text{Yarn} - \text{OH} + \text{NaOH} \rightarrow \text{yarn}{-}\text{O}^{-}\text{NA}^{+} + \text{H}_2\text{O} + \text{impurities} \quad (1)$$

The alkaline environment created by the NaOH solution disrupts both intermolecular and intramolecular hydrogen bonds within the cellulose structure (El Seoud et al. 2019). This disruption enhances the separation of cellulose yarns and heightens their reactivity, making them more suitable for subsequent processing steps like dissolution, modification, or regeneration (Sen Wang et al. 2016; Liyanage et al. 2021). This pre-treatment represents a fundamental step in the broader realm of cellulose yarn processing, optimizing their utility for a variety of industrial and research applications (Gassan and Bledzki 1999).

It is important to investigate and comprehend the impact of alkali treatment on cellulose yarns, as it opens avenues for producing high-quality textiles across diverse industries. Many studies have reported reduced moisture absorption in yarns following NaOH treatment, thereby mitigating the inherent hydrophilic nature of natural cellulosic materials compared to untreated ones (Mwaikambo and Ansell 2002; Baghaei et al. 2014). For instance, hemp treated with a 5 wt.% NaOH solution showed a notable reduction in lignin and pectin content, along with a 4.4% increase in the crystallinity index, as observed by Beckermann and Pickering (2008). This heightened crystallinity index is attributed to the removal of lignin and pectin, allowing for more efficient cellulose chain packing (Tanasă et al. 2020).

The inherent insolubility of cellulose in both water and most organic solvents can be attributed to two key factors. Firstly, cellulose chains are organized into highly crystalline micro-fibrils (Pinkert et al. 2009), and secondly, the presence of intra- and inter-chain hydrogen bonds formed between hydroxy groups (Gross and Chu 2010; Chen et al. 2015). As a result cellulose dissolution necessitates the disruption of its hydrogen bond network, a process that can involve prior chemical modifications (Sen et al. 2013). Furthermore, Medronho and Lindman (2014) demonstrated that the degree of polymerization (DP) significantly affects the dissolution of cellulose. Higher DP leads to increased chain entanglement and

stronger intermolecular hydrogen bonding, which enhances structural rigidity and resistance to solvent penetration.

The environmental concerns associated with traditional organic solvents can potentially be mitigated by substituting them with ionic liquids (ILs). Recent studies (Abushammala and Mao 2020; Bodachivskyi et al. 2020) highlight the significant promise of ILs as cellulose solvents. ILs are a category of organic salts characterized by a low melting point, typically below 100 °C (Walden 1914; Matandabuzo and Ajibade 2018). One of their notable attributes is their minimal vapour pressure, leading to reduced emissions of harmful gases, making them safer for handling and recycling (Huber et al. 2012). By combining various anions and cations, a diverse range of ILs can be synthesized, potentially replacing conventional solvents in numerous applications (Duchemin et al. 2009; Shamsuri et al. 2021). These properties have led to the exploration of ILs as promising solvents in various scientific and technological fields, including their application in cellulose dissolution for the creation of all-cellulose composites (ACCs) (Huber et al. 2012; Abushammala and Mao 2020; Baghaei and Skrifvars 2020; Victoria et al. 2022).

In the process of recovering cellulose from IL solutions, coagulation agents like water and ethanol are often employed to remove the ILs (Cao et al. 2010; Lopes et al. 2017), followed by a drying process to evaporate the coagulation agents. Despite decades of research into the use of ILs for cellulose dissolution, the underlying mechanisms remain not fully understood. Some fundamental studies have examined the kinetics and rheology of cellulose dissolution in ILs, with recorded rheological activation energies (E_a) ranging from 46 to 70 kJ/mol, depending on the IL and cellulose concentration (Gericke et al. 2009; Budtova and Navard 2015; Druel et al. 2018). Recent research suggests that the dissolution of cellulose in ILs follows an Arrhenius behaviour (Liang et al. 2020; Albarakati et al. 2023; Alrefaei et al. 2023). Notably, the activation energies (E_a) for the dissolution of (natural/untreated) cotton, hemp and flax cellulose have been determined to be 96 ± 3 kJ/mol 78 ± 2 kJ/mol (Liang et al. 2020; Alrefaei et al. 2023), and 64 ± 5 kJ/mol (Albarakati et al. 2023), respectively. However, research on alkali-treated yarns using a similar methodology is yet to be found, and of key importance investigating the reason for the different activation energies of these yarns.

This study investigates the dissolution behavior of both raw and NaOH-treated cellulose plant-based yarns in 1-ethyl-3-methylimidazolium acetate ([EMIM][OAc]). The primary objective is to examine the relationships between plant composition, molecular weight, and crystallinity, and to explore how these factors influence the dissolution behaviour, characterized by the dissolution activation energy. Plant composition, including cellulose, hemicellulose, lignin, and pectin, may affect the activation energy (Sgriccia et al. 2008). Our hypothesis though, is that the molecular weight of the cellulose chains is the dominant factor in determining the rate of dissolution and the dissolution activation energy itself.

We utilize optical microscopy (OM) to assess changes in morphology resulting from different processing temperatures and/or times. The dissolution progress is quantified using multiple methodologies based on the OM findings. We demonstrate the applicability of time–temperature-superposition (TTS) and the independence of the dissolution activation energy (E_a) from the particular quantification method. The proposed method in this study involves treating the yarns to alter their compositional balances and molecular weight, with the findings offering valuable insights and novel techniques for investigating other cellulose-based materials and yarns. Additionally, this method significantly contributes to the fabrication of all cellulose composites (ACCs). These materials offer distinct advantages: biodegradability, sustainability, and compatibility with cellulose-based products (Huber et al. 2012; Baghaei and Skrifvars 2020; Victoria et al. 2022). By integrating alkali treatment into the manufacturing process, researchers have the potential to develop enhanced, resilient, and adaptable ACCs, thereby expanding the scope of their applications across diverse industries. The impact of the alkali treatment on dissolution speed is systematically examined by tracking the dissolution behaviour of hemp, flax, and cotton yarns both before and after undergoing the alkali treatment. Our hypothesis is that all these effects can be explained primarily by the changes in molecular weight of the cellulose chains within the yarns, and that it is the cellulose molecular weight that determines the dissolution activation energy.

Materials and methods

Materials

In this study, three distinct varieties of cellulosic yarns served as the sources of cellulose. Hemp, obtained from Etsy, Inc. in the United Kingdom, was utilized in the form of continuous yarns with an approximate diameter of 400 µm, corresponding to a linear density of 180 denier. Natural cotton and flax yarns, procured from Airedale Yarns in Keighley, UK, were employed as continuous yarns, with approximate diameters of 300 and 500 µm, respectively, and estimated linear densities of approximately 120 denier (for cotton) and 250 denier (for flax). All yarns were of textile grade, typically used for weaving and knitting applications such as apparel fabrics. The ionic liquid 1-ethyl-3-methylimidazolium acetate ([EMIM][OAc], purity > 98%) was purchased from Proionic GmbH (Grambach, Austria). Water content of the IL (< 0.2%) was measured with a Karl Fischer titration device (899 Coulometer, Metrohm U.K. Ltd., UK).

Epoxy resin was used to embed dried samples for cross-sectional observation under an optical microscope. The samples were positioned perpendicularly to the polishing surface at the bottom of a Teflon circular container, into which the resin was poured. The setup was left to cure for 24 h. After which the embedded samples were ground and polished using a polishing machine (STRUERS ROTOPOL-11, Struers Ltd., UK) to achieve a thickness of approximately 3 cm. Finally, further image processing was performed using 'ImageJ' software.

Methods

Alkali treatment with NaOH and cellulose processing with [EMIM][OAc]

Natural yarns were immersed in a solution containing 4% (wt.) aqueous NaOH for 3 h. The treatment reaction was carried out at 21 °C with 6.26 wt.% of the material. Treated samples were then washed with distilled water to neutral pH and left to air-dry at 21–22 °C for 48 h. The testing was conducted in a controlled laboratory environment, including regulated humidity and temperature, to minimize random errors.

Ten separate yarn loops were then fixed onto 8 × 8 cm PTFE picture frames and transferred into PTFE dishes containing 50 mL of [EMIM][OAc], preheated to the desired temperature and containing 2.44 wt.% of the yarns (see Fig. 1). In this paper we show results for four new yarns, mercerised hemp, natural and mercerised cotton and mercerised flax, with mercerised hemp being used to describe the analysis procedures in detail. Natural hemp results were taken from our previously published paper (Alrefaei et al. 2023) while the natural flax results were taken from the published work of (Albarakati et al. 2023). So, we then have results for six yarns: natural hemp, alkali-treated hemp, natural cotton, alkali-treated cotton, natural flax, and alkali-treated flax. These variations allowed for a comparative investigation into the effects of both yarn type and alkali treatment on the dissolution behaviour in the ionic liquid medium.

The PTFE dishes were placed in a vacuum oven (Shellab 17L Digital Vacuum Oven SQ-15VAC-16, Sheldon Manufacturing, Inc., USA) following the studies by (Lovell et al. 2010; Gschwend et al. 2020; Hawkins et al. 2021; Albarakati et al. 2023), and yarns were treated with various time intervals (ranging from 0.25 to 6 h) at four distinct target temperatures (30 °C, 35 °C, 40 °C, and 50 °C). Yarns were then coagulated under gently running water at 20 °C that was sustained for 24 h to remove any residual [EMIM][OAc]. Yarns were then left to air dry for 48 h at 21 °C.

The cross-section of the yarns was revealed by embedding the partially dissolved yarns in epoxy resin, and then these were imaged in reflection using an optical microscope. Optical micrographs revealed two distinct regions. An undissolved inner core surrounded by a skin of dissolved and coagulated material. The width of this outer skin (x) was determined by measuring both the inner diameter and the total diameter of the processed yarn. This was done four times for each partially dissolved yarn and then repeated for four yarns made under the same conditions of time and temperature giving sixteen repeat measurements in total. On the other hand, the coagulated fraction CF of yarns is determined by measuring the total area of the fibrous cross-section and the area of the central yarn. Sixteen measurements were taken to calculate the means and standard errors of the width of the outer skin (x) of the dissolved yarn and the calculated coagulated fraction CF. Previous

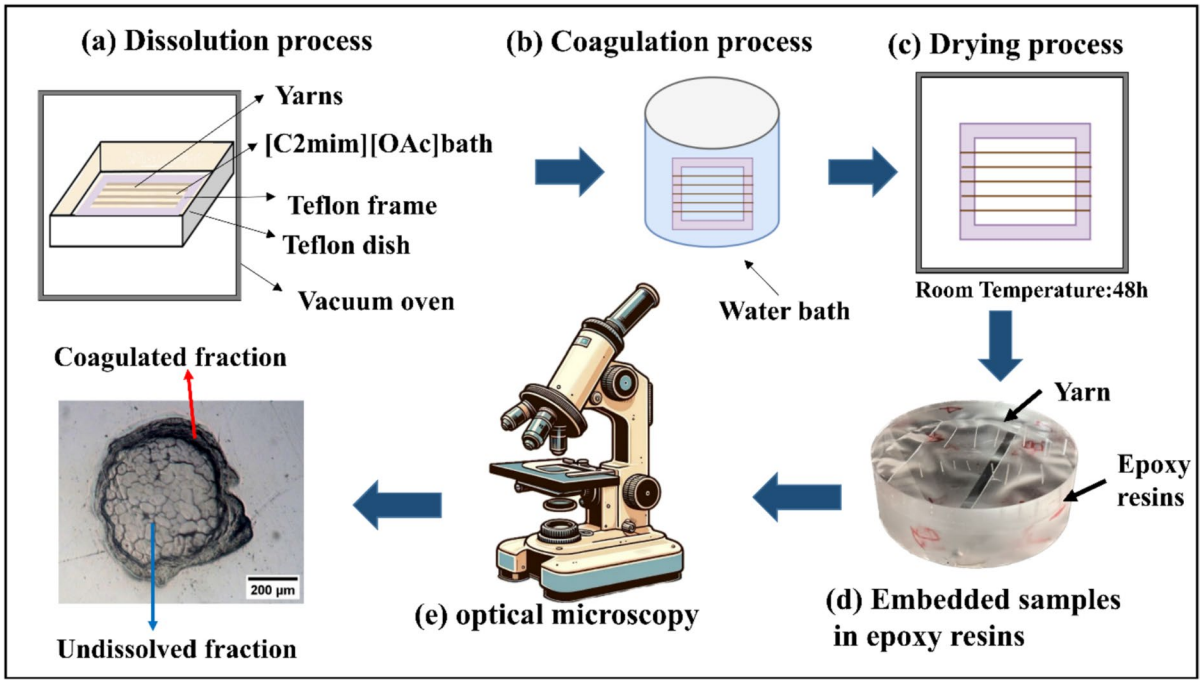

Fig. 1 The preparation process of partially dissolved yarns: **a** Dissolution process within the IL, **b** Coagulation process using a water bath as anti-solvent, **c** Drying process, **d** Embedded yarns in epoxy resins, **e** Using an optical microscope to investigate cross-sections of the processed samples

studies have confirmed the reliability of this measurement technique in quantifying yarn dissolution for materials such as flax (Hawkins et al. 2021) and cotton, yielding repeatable results (Liang et al. 2020). For the exploration of the treated yarn morphology, especially in examining cross-sections of partially dissolved materials, an optical microscope (BH2-UMA, Olympus Corporation, Japan) operating in reflection mode was employed.

X-ray diffraction

X-ray Diffraction (XRD) was employed to characterize the crystalline structure of the various cellulosic samples using a DRONEK 4-AXES XRD machine (Huber Diffraktionstechnik GmbH & Co. KG, Germany) in transmission mode. 2θ scans were conducted with the following parameters: 2θ ranging from 5° to 40°, with a step (resolution) of 0.2°, each step lasting 50 s. X-rays were generated with a wavelength (λ) of 0.154 nm using Cu-Kα radiation at an operating voltage of 40 kV and a current of 30 mA. First, a scan without a sample was carried out and this was then subtracted from each set of results to correct for background/air scattering. Although there are a variety of methods in the literature for analyzing cellulose crystallinity, one frequently used approach is peak convolution, where a number of peaks associated with each Bragg peak are optimised to fit the overall diffraction pattern. More recently, French (2020) has recommended a Rietveld method, which more accurately reflects all the possible crystalline diffraction peaks rather than using a broad single amorphous peak as often used. We have followed this recommendation and have made use of the free MAUD software (Materials Analysis Using Diffraction—https://luttero.github.io) to fit our X-ray diffraction results. All the results fitted well to a cellulose Iβ unit cell (main Bragg peaks at 14.8° ($1\bar{1}0$), 16.7° (110), and 22.7° (200) French (2014)) plus a number of other crystalline peaks. Figure S1 presents a typical fit to the X-ray diffraction data collected for the raw natural hemp.

Molecular weight and carbohydrate composition analysis

The molecular weight analysis involved treating cellulosic samples (hemp, cotton and flax) following a standard protocol for cellulose labelling. This process included soaking the samples in a shaking water bath at 40 °C for 7 days, solvent exchange from water to ethanol, and then to DMAc with a 12-h soaking period. The samples were fully dissolved in DMAc/LiCl to achieve a solution with 9 wt. % of the samples, followed by dilution with DMAc before injection into a GPC machine. Carbohydrate composition was determined by cryogenically milling samples in a Retsch mill for 10 min, followed by drying at 40 °C in a vacuum oven. Lignin content was measured using the acetyl bromide spectrophotometric method based on Iiyama and Wallis (1988) with modifications from Hatfield et al. (1999). About 20 mg of dry, milled sample was treated with 1 mL of freshly prepared 25% acetyl bromide in glacial acetic acid, sealed, and incubated at 70 °C for 30 min. After cooling, 72 mg of sodium hydroxide and 34.7 mg of hydroxylamine hydrochloride were added to stop the reaction and neutralize bromine. The volume was adjusted to 10 mL with glacial acetic acid, and absorbance was measured at 280 nm. The hemicellulose content was determined by acid methanolysis, following the method described by Sundberg et al. (1996). Samples (5–10 mg) were treated with 2 mL of 2 M HCl in anhydrous methanol, incubated at 100 °C for 3 h, then neutralized with pyridine. The hydrolysate was dried under nitrogen, reconstituted in solvent (acetonitrile or water), and analyzed by gas chromatography with pulsed amperometric detection to quantify monosaccharides, providing detailed hemicellulose composition.

Results and discussion

Yarn surface morphology using optical microscopy

Optical microscopy (OM) plays a crucial role in capturing morphological images of yarns, both in their pristine state before treatment with NaOH and following dissolution using [EMIM][OAc] ionic liquid. OM provides a rapid means of assessing the extent of yarn dissolution due to the noticeable difference between undissolved and coagulated material when observed using a microscope, as shown in Fig. 2.

The process of quantifying the coagulated fraction in these dried, partially dissolved yarns adhered to the methodology previously reported by Alrefaei et al. (2023) for natural hemp yarns. In this study, the same procedures were employed to assess the dissolved component of the processed yarns. Following the drying of samples, each set of four specimens was embedded in epoxy resin and polished to expose the cross-section micromorphology, as depicted in Fig. 1d. After the processing, optical micrographs revealed two distinct regions, as seen in Fig. 2c. The inner fibrous core was enclosed by a visibly different outer layer, consisting of the coagulated cellulosic material.

In Fig. 2a, an optical micrograph shows an untreated natural hemp yarn embedded within epoxy resin, while Fig. 2b represents a cross-section of the hemp sample, showing the effects of the alkali treatment. Figure 2c, d display samples post-partial dissolution with an ionic liquid (IL). Each yarn comprises a loose arrangement of numerous tiny hemp microfibers, bundles closely packed side by side. The measurement of the width of the outer skin (x) and the fraction of the encompassing coagulated cellulose, calculated within the epoxy (CF), were accomplished using image processing software (Image J). The corresponding Eqs. (2) and (3) were employed to derive the values for (CF) and (x), as indicated below.

$$x = (D_0 - D_i)/2 \tag{2}$$

where D_0 and D_i represent the total outer diameter of the whole sample and the diameter of the central region of these samples, which are described in Fig. 2c.

$$CF = \left(A_0 - A_i\right)/A_0 \tag{3}$$

where A_0 represents the total cross-sectional area of the entire sample, while A_i is the cross-section area of the core undissolved fraction of samples, as shown in Fig. 2d. The outer layer is presumed to consist of cellulose that has been dissolved and coagulated.

So, in the case of the partially dissolving process of these yarns, the densely packed arrangement of yarns hinders the ionic liquid (IL) from infiltrating the fibrous core. Instead, as dissolution time increases, the distinct boundaries between the

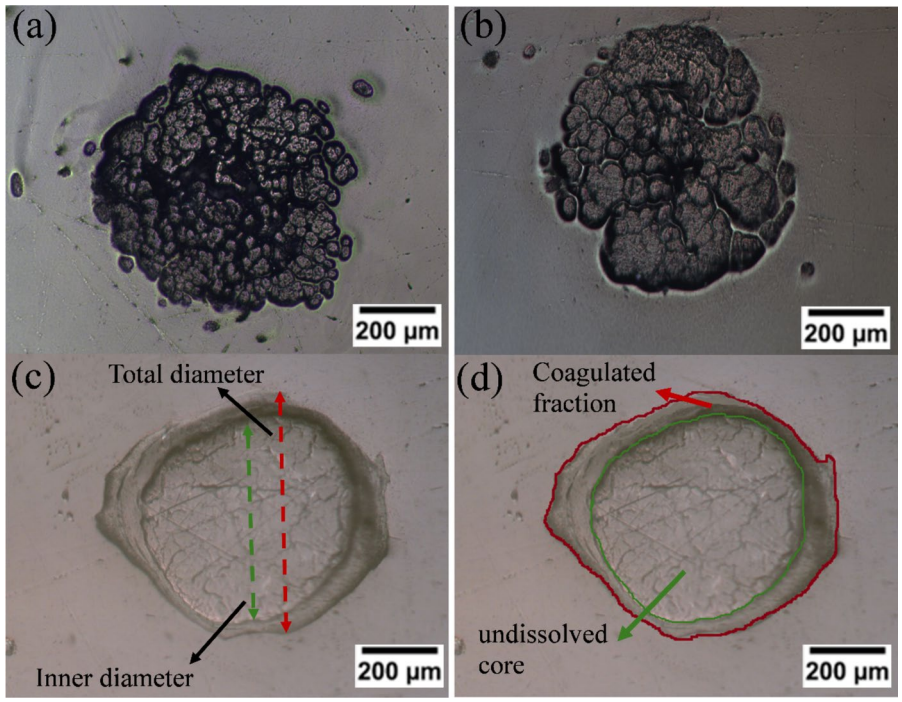

Fig. 2 **a**: A cross-sectional view of natural hemp material observed under an optical microscope. **b**: A cross-sectional view of alkali-treated hemp material. **c**: A cross-sectional view of an alkali-treated hemp yarn that has been partially dissolved following treatment with [EMIM][OAc], the width of the outer skin of coagulated material through measuring total outer (indicated with the red arrow) and inner core (indicated with the green arrow) diameters **d**: To determine the coagulated fraction (*CF*) of an alkali-treated hemp yarn, measure the total area of the fibrous cross-section (indicated by the red arrow) and the area of the central yarn (indicated by the green arrow). The scale bars represent 200 microns

dissolved and undissolved portions migrate toward the centre, as shown in Fig. S2, which provides micrographs of treated yarns at 40 °C for varying durations (0.5 h, 1h, 2h, and 4h). Notably, the structure of the undissolved segment closely resembles the composition of the untreated yarns, underscoring this observation. This material exhibits an undissolved central core surrounded by a dissolved and coagulated region. Furthermore, alternative sample preparation methods may provide additional insight into the morphological evolution of these yarns. In particular, the tubular embedding technique described by Boylston et al. (1991) offers a rapid and effective approach for embedding textile fibres for microscopic analysis. Implementing such a method in future work could help preserve fibre alignment and structural integrity during sectioning, thereby improving the visualization of partially dissolved regions.

Time–temperature superposition

The two parameters, the coagulation fraction *(CF)*, and the width of the outer skin (*x)* of the processed yarns, were measured by optical microscopy. These parameters were used in analysing data at different temperatures and times, as shown in Figs. 3 and 5, for treated hemp. We found that the coagulated fraction (*CF*) and the width of the outer skin (*x*) increased as both processing time and temperature were raised, as shown in Figs. 3a and 5a, respectively. The measurements align with the earlier observations made through the microscope images in Fig. S2, showing that as the processing time and temperature are raised, the values of *CF* and *x* also increase.

A closer examination of the curves in Fig. 5a revealed the potential use of a time–temperature equivalence method to construct a master curve at each temperature, a practice routinely applied

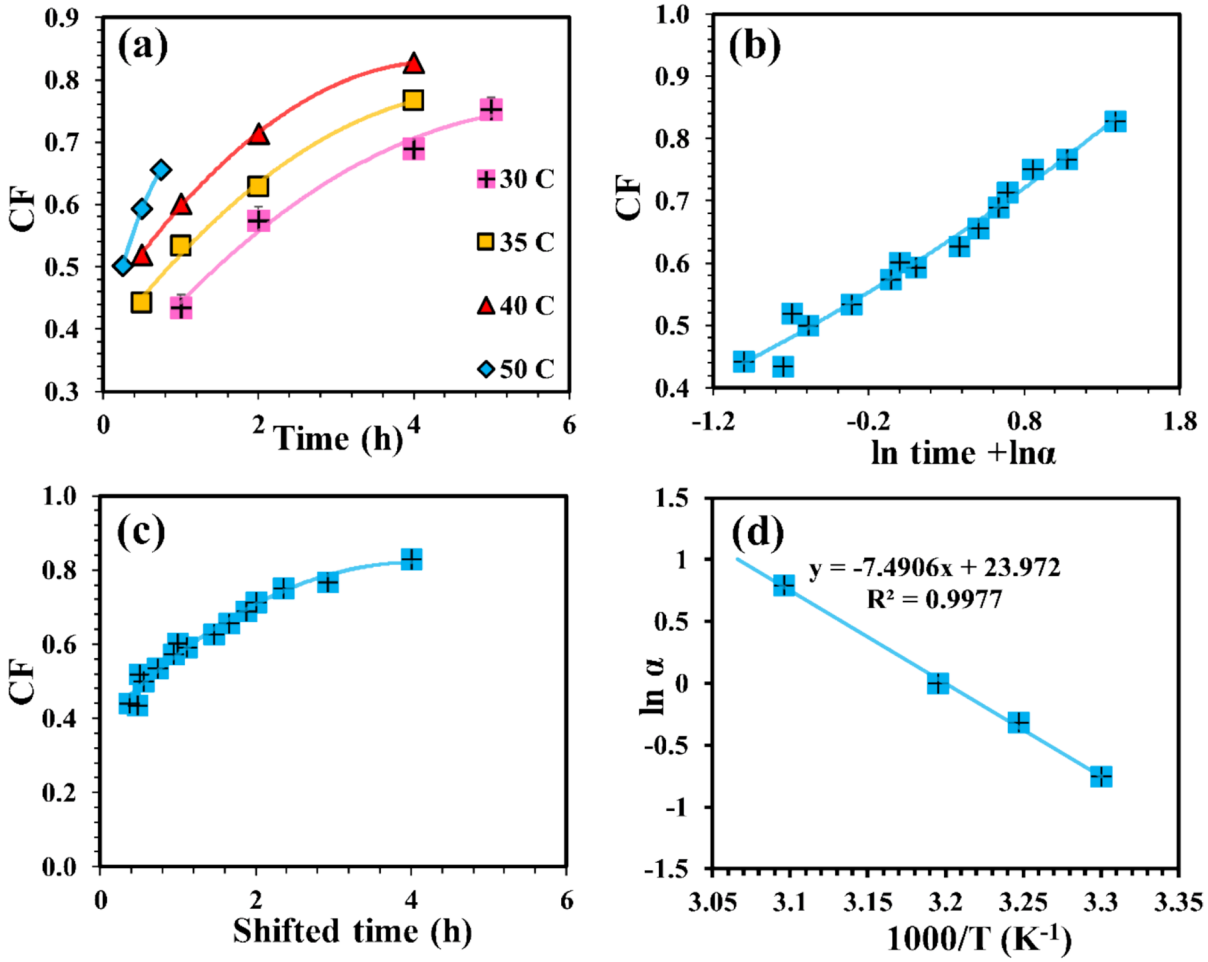

Fig. 3 **a** Plotting the coagulated fraction (*CF*) of treated hemp against dissolution time for all dissolution temperatures, with the red triangle representing the reference temperature of 40°C and guiding lines provided to aid visualization. **b** Representing (*CF*) as a function of dissolution time for all temperatures using ln time, the line is a second-order polynomial fit to the data. **c** Master curve illustrating the impact of both time and temperature on (*CF*); the line represents a second-order polynomial fit. **d** Arrhenius plot displaying the relationship between the shift factors (ln α) and temperature, with a linear fit to the data depicted by the line. All the errors were computed, though, in certain instances, they were smaller than the size of the data points

in the analysis of rheological data, and as we have employed in our prior studies involving natural hemp, flax, and silk (Zhang et al. 2021; Albarakati et al. 2023; Alrefaei et al. 2023).

To obtain a master curve at the chosen reference temperature of 40 °C, all data points were shifted in ln (time) towards this temperature to form a single master curve, as shown in Figs. 3b and 5b. The procedure was as follows.

A scaling factor ($\alpha_{Tref,T}$) was determined using the equation:

$$t'_{Tref} = \alpha_{Tref,T} t_T \quad (4)$$

where t'_{Tref} represents the shifted time at a reference temperature $T_{ref,}$, $\alpha_{Tref,T}$ is the scaling factor that takes the time from a measured temperature T to the reference temperature T_{ref}, and t_T is the original time at the measured temperature. When expressed in natural logarithms, this equation becomes:

$$\ln(t'_{Tref}) = \ln(\alpha_{Tref,T}) + \ln(t_T) \quad (5)$$

Initially, data were displayed in natural logarithmic time (ln (t)). The data at 40 °C was fitted using a polynomial function to guide the shifting process visually. Each dataset dependent on temperature was horizontally shifted by an amount of ln ($\alpha_{Tref,T}$) to overlap with the reference data.

Subsequently, a polynomial function was used to fit all data points. Minor adjustments were made to shift factors to maximize the R^2 value of this polynomial fit. Figures 3b and 5b depict data after shifting to 40 °C as a reference temperature, while Figs. 3c and 5c present the real time master curves following this shift. Notably, the master curves derived from Fig. 5c, when presented in terms of linear time, reveal that the dissolution rate initially proceeds at a relatively fast pace and then gradually slows down with time. In order to explore the connection between dissolution time and temperatures, the shift factors were plotted against the inverse of their dissolution temperatures, as shown in Figs. 3d and 5d. This analysis yielded linear relationships, indicative of Arrhenius-type behaviour in the dissolution dynamics. This enabled the calculation of the dissolution activation energy for the processed cellulosic yarns using the Arrhenius equation.

$$\alpha_{Tref,T} = Ae^{-E_a/RT} \tag{6}$$

Here, E_a represents the dissolution activation energy, A is the Arrhenius pre-factor, R denotes the gas constant, T signifies temperature, and $\alpha_{Tref,T}$ is the scaling factor at temperature (T). The dissolution activation energy E_a of the yarns in [EMIM][OAc] was determined from the slopes in Figs. 3d and 5d. The resulting average value of the dissolution activation energy E_a of treated hemp yarn is approximately 68 ± 2 kJ/mol, which is lower than our previously published work which determined a value for un-treated natural hemp of 78 ± 2 kJ/mol (Alrefaei et al. 2023). The uncertainty value comes from using the LINEST function in Excel on Fig. 5d. The same analytical approach was employed for evaluating additional treated yarns, including cotton and flax, alongside un-treated cotton, as illustrated in Figs. S3, S4, and S5. The findings indicate that the dissolution activation energies differ among various materials. Specifically, for treated cotton and flax, the activation energies were determined to be 64 ± 2 kJ/mol and 55 ± 3 kJ/mol, respectively. In contrast, un-treated cotton exhibited a higher activation energy of 84 ± 4 kJ/mol, while natural flax showed an activation energy of 64 ± 5 kJ/mol (Albarakati et al. 2023).

Figure 4a compares the master curves at a reference temperature of 40 °C, for natural hemp and treated hemp. It is seen that the treated hemp dissolves significantly faster compared to the natural yarn. To calculate the relative dissolution rate before and after the alkali treatment, we shifted the master curve for treated hemp, represented in Fig. 3c, to overlap with the master curve of un-treated (natural) hemp yarns, as reported in our previous work (Alrefaei et al. 2023). This adjustment allows us to

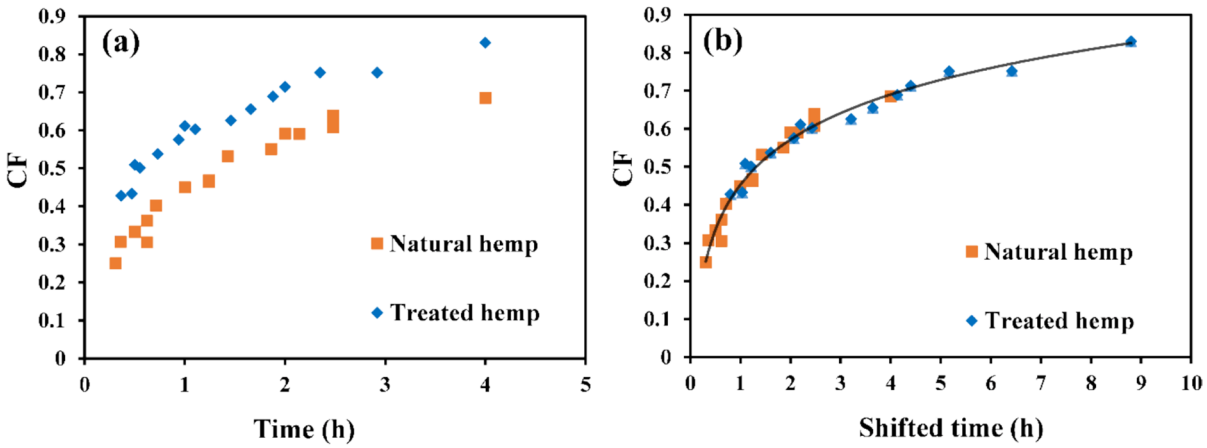

Fig. 4 **a** Master curve presenting the coagulation fraction *CF* across all temperatures for natural and treated hemp yarns. Each data set uses 40 °C as a reference temperature. **b** Overlaying the master curve of treated hemp with that of un-treated (natural) hemp yarns

measure the relative dissolution rate between untreated hemp yarns and treated hemp yarns.

The amounts by which each material's master curve must be shifted to create Fig. 4b act as a direct measurement of the relative dissolution rates. The data for natural hemp must be scaled by a factor $\alpha = 2.2$ in order to overlap with the treated hemp master curve, revealing that the dissolution rate for the treated yarns is 2.2 times faster.

This observed difference in the relative dissolution rates between treated and natural hemp yarns is also shown in the other two yarns, namely flax and cotton. Figure S6 shows similar results to Fig. 4, while Table 1 below summarises the three relative dissolution rates. Notably, the relative dissolution speed of treated yarns surpasses that of natural yarns in all cases. For instance, in treated cotton, the relative speed rate is 5.0 times higher than that

Table 1 The relative dissolution rate of hemp, cotton, and flax (alkali-treated: natural)

Material	The relative dissolution rate alkali-treated: natural
Hemp	2.2
Cotton	5.0
Flax	4.3

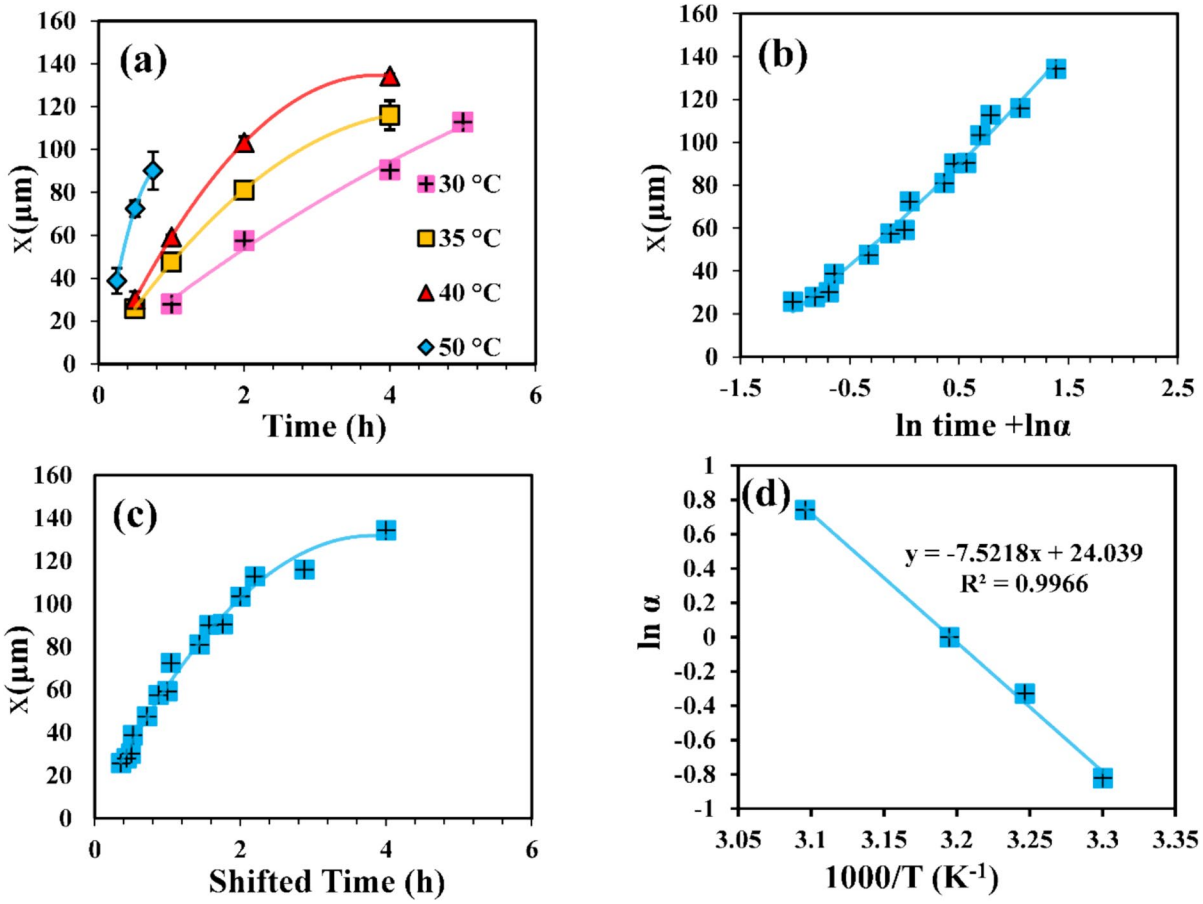

Fig. 5 **a** Plotting the width of the outer skin (x) for alkali-treated hemp against dissolution time for all dissolution temperatures, with guiding lines for visual reference. **b** x as a function of dissolution time for all temperatures shifted to a reference temperature of 40 °C expressed in ln time, with a second-order polynomial fitted to the data. **c** A master curve illustrating the combined impact of both time and temperature on the width of the outer skin, with a second-order polynomial fit denoted by the line. **d** An Arrhenius plot displaying the relationship between the shift factors ($\ln_\alpha$) and temperature, with a linear fit to the data

of natural cotton. Similarly, treated flax exhibits 4.3 times increase compared to its natural state. We observed that the common finding across materials studied here is that the relative speed rate of alkali-treated yarns is consistently higher than that of natural yarns.

The rate of increase in both coagulation fraction (*CF*) and the width of the outer skin (*x*) exhibited a slowing down over time, as clearly indicated by the master curves illustrated in Figs. 3c and 5c. A plausible interpretation for this phenomenon is that with the extension of processing time, a growing fraction of the outer cellulose hinders further dissolution. This may function as a protective barrier, effectively isolating the inner core from the surrounding solvent (Hawkins et al. 2021; Liang et al. 2020).

Diffusion method

In this study, we employed a method, described in our previous work, to monitor the growth in the width of the outer skin of the coagulated region (Alrefaei et al. 2023). The examination is based on the information presented in Fig. 5c, which illustrates the growth of the width of the outer skin over time. Analysis of the time–temperature superposition (TTS) data indicates a decreasing growth rate for this outer region over time. In Fig. 6a, the width of the outer skin of the outer dissolved and coagulated region is plotted against the square root of time, $\sqrt{t}$, where t signifies the dissolution time in hours. The graph shows that a linear dependence is seen when the data is plotted in this way. This observation suggests that the growth of coagulated regions within the system is controlled by diffusion.

In terms of one-dimensional diffusion, the following relationship is established:

$$\mathrm{r} \sim \left\langle r^2 \right\rangle^{1/2} = (2D)^{1/2} * \mathrm{t}^{1/2} \tag{7}$$

where (r) represents the distance diffused over time (t) for a molecule with a self-diffusion coefficient (D) (Mazo 2002). Here, (r) is utilized to model the width of the outer skin of the coagulated region, or in other words, the depth of penetration of the ionic liquid into the yarn after a given time t. It should be noted that we are making the simplifying assumption that the ionic liquid is diffusing in just one dimension, namely the penetration depth into the fibre. The slope of the straight line in Fig. 6a provides a (D) value of 6.16 $\times 10^{-13}$ m^2/sec at 40 °C.

In this context, time–temperature superposition plots were generated employing the same approach explained earlier. Four master curves were constructed since the system includes four temperatures (30, 35, 40, and 50 °C) by choosing a different reference temperature within the system for each analysis. At each reference temperature, the width of the

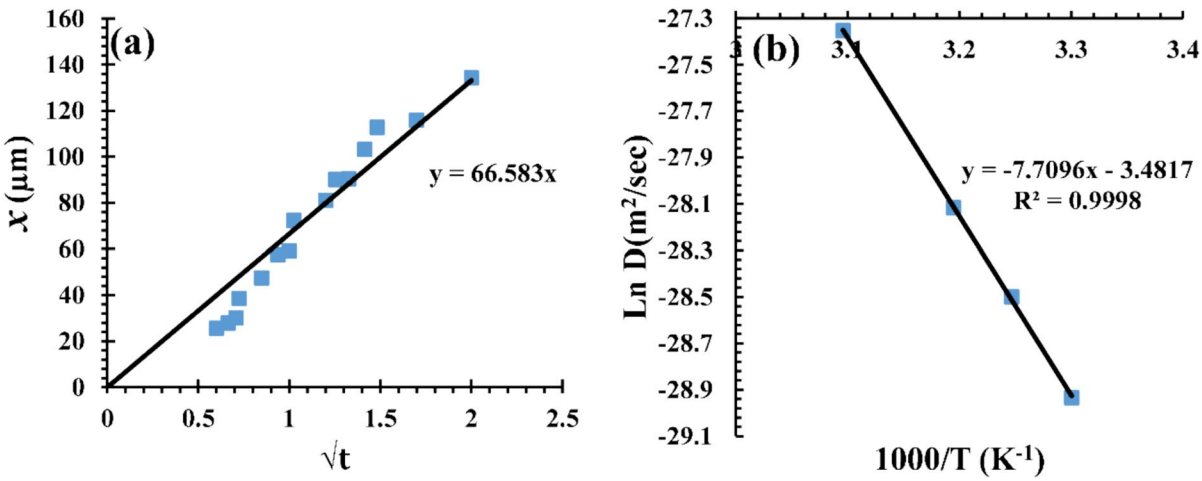

Fig. 6 **a** Plot the width of the outer skin of processed yarns at 40 °C as a function of $\sqrt{t}$. **b** The natural log of the self-diffusion coefficient (*LnD*) of the ionic liquid [EMIM][OAc] in the yarns as a function of temperature, showing Arrhenius behaviour. Errors bars are smaller than data points used

outer skin increase was calculated using Eq. (3). Figure 6a represents the correlation between the outer skin growth and the square root of time of the master curve at a reference temperature of 40 °C.

The self-diffusion coefficients acquired at each temperature within this system are outlined in Table S1. This information presented in Fig. S7 and Table S1 was utilized to determine the relationship between the natural logarithm of D and the inverse temperature. The data obeys Arrhenius behavior, so similar to the activation energies of dissolution discussed earlier, the slopes obtained from each linear fit of the natural logarithm of D versus inverse temperature, as illustrated in Fig. 6b, were employed to ascertain the activation energy using the following equation:

$$\ln D = \ln D_0 - E_{\alpha,D}/RT \tag{8}$$

where D_0 represents the pre-exponential factor, while $E_{\alpha,D}$ represents the activation energy of diffusion. The calculated activation energy of diffusion using Eq. (8) closely aligns with that of the dissolution determined earlier using TTS, with a value of 64 ± 1 kJ/mol for treated hemp yarns.

Table S2 summarises a typical set of results for the dissolution activation energy for mercerised hemp yarns obtained from the methods (epoxy resin, and diffusion analysis). This gave three parameters that could be followed with time and temperature, and all showed TTS. These were the growth of the width of the outer skin (x), the coagulation fraction CF, and the calculated diffusion coefficients (D). All were used to calculate the average dissolution activation energy (E_a) for treated hemp yarns. It can be seen that these parameters yielded excellent agreement, resulting in a final average calculated dissolution activation energy (E_a) of 63 ± 2 kJ/mol. This indicates that the activation energies are independent of the quantifying parameter used to track dissolution.

A comparison of six different natural and alkali-treated plant yarns

In the following section we investigate the effect of composition, crystallinity and molecular weight on dissolution activation energy by combining the four yarns investigated in this current study, with the two previously published works of our group, giving in total six different yarns. The mercerised hemp described in detail above, the natural hemp from our previous publication, natural flax results from (Albarakati et al. 2023), which is the same flax yarn treated as part of this study (Fig. S4) and both natural and treated cotton from this study (Figs. S3 and S5).

A comparison of these current findings with our previous investigation on natural hemp (Alrefaei et al. 2023), reveals a reduction in the activation energy (E_a) for the treated yarns, measuring 68 ± 2 kJ/mol, in contrast to the prior value of 78 ± 2 kJ/mol reported for natural yarns. Additionally, dissolution activation energies were determined to be 64 ± 2 kJ/mol and 55 ± 3 kJ/mol for treated cotton and flax, respectively, as opposed to 84 ± 4 kJ/mol in this work and 64 ± 5 kJ/mol as reported previously by (Albarakati et al. 2023) for their counterparts in their natural state. All these results are summarised in Table 2.

To explore the potential underlying microscopic causes behind the differences in dissolution activation energies between the natural and treated states of these cellulosic yarns (hemp, flax and cotton), the composition and molecular weight were determined, and are given in.

Table 3. This displays the molecular weight, lignin concentration, and carbohydrate composition of the hemicelluloses found in the yarns.

The correlation between lignin content and the dissolution activation energy of cellulosic yarns (hemp, cotton, and flax) before and after the alkali treatment was investigated, and a plot can be seen in Fig. 7a indicating no clear correlation. Similarly, no clear correlation was found between the carbohydrate composition, including glucose, galactose, and galacturonic acid of the hemicelluloses, and dissolution activation energy across all compositions, see Fig. 7b–d. These four graphs strongly suggest that variations in the composition of cellulosic yarns do not significantly impact the dissolution activation

Table 2 Average dissolution activation energy of the cellulosic yarns (hemp, cotton, and flax) before and after the alkali treatment

Material	Natural yarns	Alkali-treated yarns
Hemp	78 ± 2 kJ/mol	63 ± 2 kJ/mol
Cotton	84 ± 4 kJ/mol	64 ± 2 kJ/mol
Flax	64 ± 5 kJ/mol	55 ± 3 kJ/mol

Table 3 Molecular weight, lignin concentration, and composition of hemicelluloses of the cellulosic yarns (hemp, cotton, and flax) before and after the alkali treatment

Property	Natural hemp	Treated hemp	Natural cotton	Treated cotton	Natural flax	Treated flax
Molecular weight (kDa)	530.9	383	653.1	388	369.5	293.9
Lignin content of dry sample (%)	1.4	0.45	1.29	0.45	1.54	0.6
Arabinose (mg/g)	6.17	3.14	3.94	1.76	4.31	2.36
Rhamnose (mg/g)	7.09	6.78	1.23	0.98	7.28	5.98
Xylose (mg/g)	6.69	3.24	2.08	1.36	6.89	3.21
Galacturonic acid (mg/g)	11.24	8.86	6.73	4.2	10.35	7.3
Mannose (mg/g)	24.03	8.82	null	0.31	23.6	8.33
Galactose (mg/g)	31.05	30.78	2.72	2.73	36.57	31.67
Glucose (mg/g)	141.5	128.35	156.69	140.28	185.54	130.49

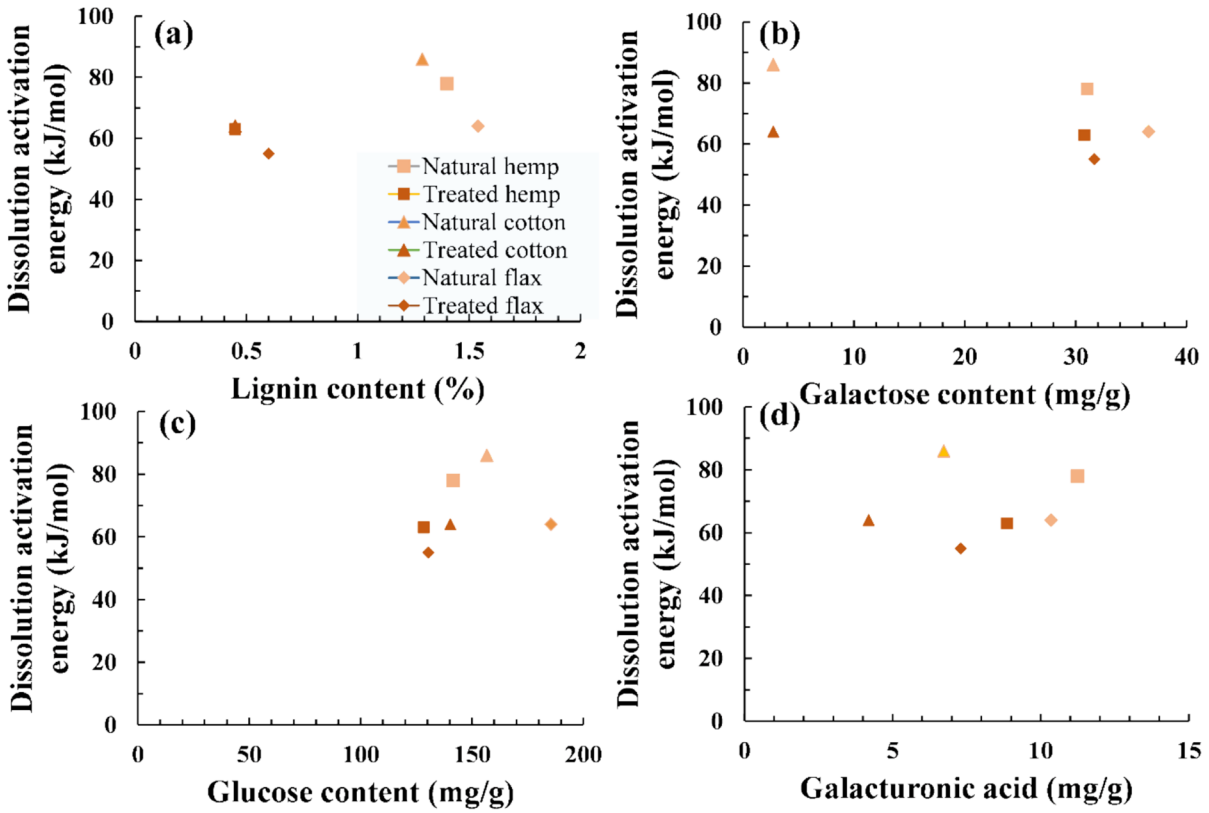

Fig. 7 **a** Lignin content, **b** Galactose, **c** Glucose, and **d** Galacturonic acid of the materials—hemp, flax, and cotton as natural and treated yarns versus their dissolution activation energy. Data taken from Table 3 using the analysis given in the Methods section

energy. Additional insights into the relationship between other hemicellulose compositions and their corresponding dissolution activation energy can be found in Fig. S8.

In terms of the crystalline structure, measurements and analysis were carried out as described earlier. No significant difference was found in the fitted crystalline structures (cellulose Iβ) for the three natural

yarns, and in addition, no noticeable changes to the crystalline structure were found after the treatment. We therefore conclude that the crystalline structure is not a key parameter in controlling the changes we have observed in the measured activation energies of the six different samples.

The final parameter to be examined was the molecular weight of the six different yarns. Remarkably, when plotting the dissolution activation energy of the six yarn states within the system against their molecular weight (M_W), a linear relationship was observed, shown in Fig. 8. This indicates the significant influence of molecular weight on the dissolution activation energy, underscoring its pivotal role in affecting the dissolution process. This holds both for the natural plant yarns and the mercerised yarns, where the molecular weight is significantly reduced, and all have a lower activation energy. The molecular weight of the cellulosic gel will affect the diffusion of the solvent molecules through it, by altering the mesh size of the polymer network, the viscosity of that cellulosic solution, and by affecting the free volume available for solvent diffusion. A study reported by (Qi et al. 2008) looked at how cellulose with different molecular weights dissolves in a solution of NaOH and urea at different temperatures. They found that the solubility of cellulose in the solution depended on temperature and molecular weight.

In comparison to natural hemp, treated hemp exhibited a notable 28% reduction in molecular weight. Consequently, our investigation suggests that the treatment procedure, characterized a significant reduction in molecular weight leads to a decrease in the dissolution energy (E_a) of cellulose in [EMIM][OAc]. This hypothesis aligns with the findings of (Qi et al. 2008) in the case of a NaOH/urea solvent system. Additionally, this outcome is consistent with observations in treated flax and cotton, where molecular weight decreases after the treatment compared to their natural state. Notably, a nuclear magnetic resonance study carried out by (Ries et al. 2014) suggested a diffusion activation energy value (E_a) of 55 kJ/mol for a saturated microcrystalline cellulose solution. This value, as depicted in Fig. S9, and highlighted by the red point, aligns with the findings of our current study, thus corroborating the reported values found here using optical microscopy. Finally, the key result of this work is that, for all our samples, the dissolution activation energy,E_a (kJ/mol), is found to be proportional to molecular weight, $E_a = 30.6 + 0.0865 \times M_W$, where M_W is in kDa.

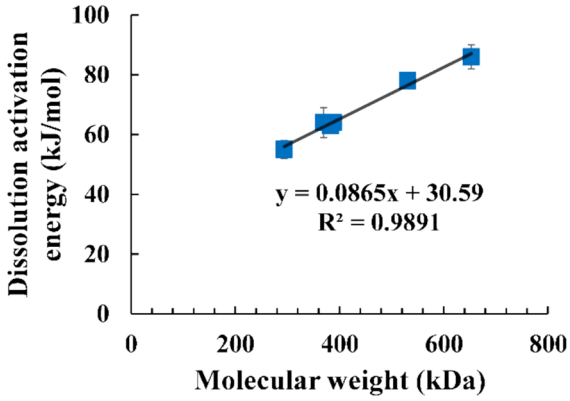

Fig. 8 Dissolution activation energy versus molecular weight of the materials—hemp, flax, and cotton as natural and treated yarns. The black line represents a linear fit to all data. All the errors were computed, though, in certain instances, they were smaller than the size of the data points

Conclusion

This study demonstrated, for the first time, that the molecular weight of natural plant-based yarns plays a central role in controlling both the dissolution rate and dissolution activation energy (E_a) in the ionic liquid [EMIM][OAc]. By applying an alkali pretreatment, using aqueous sodium hydroxide, we were able to reduce the molecular weight of three different natural yarns—hemp, cotton, and flax—and thereby investigate the microscopic origin of their dissolution behaviour. Dissolution experiments conducted across a range of time and temperature conditions revealed that the process follows the Temperature–Time Superposition (TTS) principle and can be effectively described by Arrhenius-type kinetics. Optical microscopy was employed to monitor the growth of the coagulated outer region during dissolution, which increased proportionally with the square root of time—indicating a diffusion-controlled behaviour. Three key parameters—coagulated fraction (CF), the width of the outer skin (x), and the diffusion coefficient (D)—were extracted and found to yield consistent activation energies (E_a) across all alkali-treated yarns: 63 ± 2 kJ/mol for hemp, 65 ± 2 kJ/mol for cotton, and 55 ± 3 kJ/mol

for flax. In contrast, un-treated cotton displayed a significantly higher activation energy of 86 ± 4 kJ/mol. Interestingly, neither plant composition nor crystallinity showed a clear correlation with the dissolution activation energy. Instead, a strong linear relationship was observed between activation energy and molecular weight, both in natural and alkali-treated yarns. The treatment reduced the molecular weight in all cases, resulting in faster dissolution rates and lower activation energies. We found alkali-treated hemp yarn dissolved approximately 2.2 times faster than its untreated counterpart, with similar trends observed for flax (4.3×) and cotton (5.0×). These findings establish molecular weight as the dominant factor influencing cellulose yarn dissolution in [EMIM][OAc], offering valuable insight for future processing and material optimization, for example in all-cellulose composites, using ionic liquids.

Acknowledgments The authors express their gratitude to Dr. Daniel L. Baker, Experimental Officer at the School of Physics and Astronomy, University of Leeds, for training and instructions on the experiments and to Prof. Antje Potthast, University of Natural Resources and Life Sciences, for conducting the composition measurements. They also thank Ashley Victoria, Amjad Alghamdi and Ieuan Cooper for their contributions to discussions during the research. N.A. acknowledges Taibah University for supporting his PhD scholarship.

Author contributions All authors contributed to the study's conception and design. Material preparation, data collection and analysis were mainly performed by Nora S. Alrefaei under supervision from Michael E Ries and Peter J Hine. The first draft of the manuscript was written by Nora S. Alrefaei, and all authors commented on previous versions of the manuscript. All authors read and approved the final manuscript.

Funding This research was funded by Taibah University with a PhD scholarship.

Data availability All the datasets generated during and/or analysed during the current study are freely available at [https://doi.org/10.5518/1610].

Declarations

Conflict of interest The authors declare no competing interests.

Ethical approval Not applicable.

Consent for publication All the authors have given consent for this publication, which includes text, photographs, figures and details within the text to be published in the journal "Cellulose".

References

Abushammala H, Mao J (2020) A review on the partial and complete dissolution and fractionation of wood and lignocelluloses using imidazolium ionic liquids. Polymers 12:195

Ahmad R, Hamid R, Osman S (2019) Physical and chemical modifications of plant fibres for reinforcement in cementitious composites. Adv Civ Eng 2019(1):5185806. https://doi.org/10.1155/2019/5185806

Albarakati FA, Hine PJ, Ries ME (2023) Effect of water on the dissolution of flax fiber bundles in the ionic liquid 1-ethyl-3-methylimidazolium acetate. Cellulose 30:7619–7632

Alrefaei NS, Hine PJ, Ries ME (2023) Dissolution of hemp yarns by 1-ethyl-3-methylimidazolium acetate studied with time-temperature superposition. Cellulose 30:10039–10055

Baghaei B, Skrifvars M (2020) All-cellulose composites: a review of recent studies on structure, properties and applications. Molecules 25:2836

Baghaei B, Skrifvars M, Salehi M, Bashir T, Rissanen M, Nousiainen P (2014) Novel aligned hemp fibre reinforcement for structural biocomposites: porosity, water absorption, mechanical performances and viscoelastic behaviour. Compos Part A Appl Sci 61:1–12

Balaji A, Nagarajan K (2017) Characterization of alkali treated and untreated new cellulosic fiber from Saharan aloe vera cactus leaves. Carbohydr Polym 174:200–208

Beckermann G, Pickering KL (2008) Engineering and evaluation of hemp fibre reinforced polypropylene composites: fibre treatment and matrix modification. Compos Part A Appl Sci 39:979–988

Bodachivskyi I, Page CJ, Kuzhiumparambil U, Hinkley SFR, Sims IM, Williams DBG (2020) Dissolution of cellulose: are ionic liquids innocent or noninnocent solvents? ACS Sustain Chem Eng 8:10142–10150

Boey JY, Yusoff SB, Tay GS (2022) A review on the enhancement of composite's interface properties through biological treatment of natural fibre/lignocellulosic material. Polym Polym Compos 30:09673911221103600. https://doi.org/10.1177/09673911221103600

Boylston EK, Hinojosa O, Hebert JJ (1991) A quick embedding method for light and electron microscopy of textile fibers. Biotech Histochem 66(3):122–124

Brodin M, Vallejos M, Opedal MT, Area MC, Chinga-Carrasco G (2017) Lignocellulosics as sustainable resources for production of bioplastics: a review. J Clean Prod 162:646–664

Budtova T, Navard P (2015) Viscosity-temperature dependence and activation energy of cellulose solutions. Nord Pulp Pap Res J 30:99–104

Cao Y, Li H, Zhang Y, Zhang J, He J (2010) Structure and properties of novel regenerated cellulose films prepared from cornhusk cellulose in room temperature ionic liquids. J Appl Polym Sci 116:547–554

Chen X, Chen J, You T, Wang K, Xu F (2015) Effects of polymorphs on dissolution of cellulose in NaOH/urea aqueous solution. Carbohydr Polym 125:85–91

Crini G, Lichtfouse E, Chanet G, Morin-Crini N (2020) Applications of hemp in textiles, paper industry, insulation and building materials, horticulture, animal nutrition, food and beverages, nutraceuticals, cosmetics and hygiene, medicine, agrochemistry, energy production and environment: a review. Environ Chem Lett 18:1451–1476

Druel L, Niemeyer P, Milow B, Budtova T (2018) Rheology of cellulose-[DBNH][CO2Et] solutions and shaping into aerogel beads. Green Chem 20:3993–4002

Duchemin L, Mathew AP, Oksman K (2009) All-cellulose composites by partial dissolution in the ionic liquid 1-butyl-3-methylimidazolium chloride. Compos Part A Appl Sci 40:2031–2037

El Seoud OA, Kostag M, Jedvert K, Malek NI (2019) Cellulose in ionic liquids and alkaline solutions: advances in the mechanisms of biopolymer dissolution and regeneration. Polymers 11:1917

French AD (2014) Idealized powder diffraction patterns for cellulose polymorphs. Cellulose 21:885–896

French AD (2020) Increment in evolution of cellulose crystallinity analysis. Celluose 27:5445–5448

Gassan J, Bledzki AK (1999) Possibilities for improving the mechanical properties of jute/epoxy composites by alkali treatment of fibres. Compos Sci Technol 59:1303–1309

Gericke M, Schlufter K, Liebert T, Heinze T, Budtova T (2009) Rheological properties of cellulose/ionic liquid solutions: from dilute to concentrated states. Biomacromol 10:1188–1194

Gross A, Chu J (2010) On the molecular origins of biomass recalcitrance: the interaction network and solvation structures of cellulose microfibrils. J Phys Chem B 114:13333–13341

Gschwend F, Hallett J, Brandt-Talbot A (2020) Exploring the effect of water content and anion on the pretreatment of poplar with three 1-ethyl-3-methylimidazolium ionic liquids. Molecules 25:2318

Hasan A, Rabbi M, Billah MM (2022) Making the lignocellulosic fibers chemically compatible for composite: a comprehensive review. Clean Mater 4:100078

Hatfield RD, Grabber J, Ralph J, Brei K (1999) Using the acetyl bromide assay to determine lignin concentrations in herbaceous plants: some cautionary notes. J Agric Food Chem 47(2):628–632

Hawkins J, Liang Y, Ries ME, Hine PJ (2021) Time temperature superposition of the dissolution of cellulose fibres by the ionic liquid 1-ethyl-3-methylimidazolium acetate with cosolvent dimethyl sulfoxide. Carbohydr Polym Technol Appl 2:100021

Huber T, Müssig J, Curnow O, Pang S, Bickerton S, Staiger MP (2012) A critical review of all-cellulose composites. J Mater Sci 47(3):1171–1186

Iiyama K, Wallis A (1988) An improved acetyl bromide procedure for determining lignin in woods and wood pulps. Wood Sci Technol 22(3):271–280

Kalia S, Dufresne A, Cherian BM, Kaith BS, Avérous L, Njuguna J, Nassiopoulos E (2011) Cellulose-based bio-and nanocomposites: a review. Int J Polym Sci 2011:837875

Liang Y, Hawkins JE, Ries ME, Hine PJ (2020) Dissolution of cotton by 1-ethyl-3-methylimidazolium acetate studied with time–temperature superposition for three different fibre arrangements. Cellulose. https://doi.org/10.1007/s10570-020-03576-x

Liyanage S, Acharya S, Parajuli P, Shamshina JL, Abidi N (2021) Production and surface modification of cellulose bioproducts. Polymers 13(19):3433

Lopes JM, Bermejo MD, Martín Á, Cocero MJ (2017) Ionic liquid as reaction media for the production of cellulose-derived polymers from cellulosic biomass. ChemEngineering 1(2):10

Lovell CS, Walker A, Damion RA, Radhi A, Tanner SF, Budtova T, Ries ME (2010) Influence of cellulose on ion diffusivity in 1-ethyl-3-methyl-imidazolium acetate cellulose solutions. Biomacromol 11(11):2927–2935

Matandabuzo M, Ajibade P (2018) Synthesis, characterization, and physicochemical properties of hydrophobic pyridinium-based ionic liquids with N-propyl and N-isopropyl. Z Anorg Allg Chem 644(10):489–495

Mazo RM (2002) Brownian motion: fluctuations, dynamics, and applications. Oxford University Press

Mbada NI, Aponbiede O, Ause T, Alabi A (2016) Effects of mercerization treatment on kenaf fibre (*Hibiscus cannabinus* L.). Int J Mater Eng 6(1):8–14

Medronho B, Lindman B (2014) Competing forces during cellulose dissolution: from solvents to mechanisms. Curr Opin Colloid Interface Sci 19(1):32–40

Modibbo U, Aliyu B, Nkafamiya I (2009) The effect of mercerization media on the physical properties of local plant bast fibres. Int J Phys Sci 4(11):698–704

Mohammed M, Jawad AJM, Mohammed AM, Oleiwi JK, Adam T, Osman AF, Dahham OS, Betar BO, Gopinath SCB, Jaafar M (2023) Challenges and advancement in water absorption of natural fiber-reinforced polymer composites. Polym Test. https://doi.org/10.1016/j.polymertesting.2023.108083

Moudood A, Rahman A, Öchsner A, Hasan M (2019) Flax fiber and its composites: an overview of water and moisture absorption impact on their performance. J Reinf Plast Compos 38(7):323–339

Mwaikambo LY, Ansell MP (2002) Chemical modification of hemp, sisal, jute, and kapok fibers by alkalization. J Appl Polym Sci 84(12):2222–2234

Okolie JA, Nanda S, Dalai AK, Kozinski JA (2021) Chemistry and specialty industrial applications of lignocellulosic biomass. Waste Biomass Valorization 12:2145–2169

Patil S, Mahapatra A, Gotmare VD, Patil PG, Bharimalla AK, Arputharaj A (2019) Effect of different mercerization techniques on tactile comfort of cotton fabric. Indian J Fibre Text Res 44(2):217–222

Pinkert A, Marsh K, Pang S, Staiger M (2009) Ionic liquids and their interaction with cellulose. Chem Rev 109(12):6712–6728

Qi H, Chang C, Zhang L (2008) Effects of temperature and molecular weight on dissolution of cellulose in NaOH/urea aqueous solution. Cellulose 15:779–787

Ries ME, Radhi A, Keating AS, Parker O, Budtova T (2014) Diffusion of 1-ethyl-3-methyl-imidazolium acetate in glucose, cellobiose, and cellulose solutions. Biomacromol 15(2):609–617

Sen S, Martin J, Argyropoulos D (2013) Review of cellulose non-derivatizing solvent interactions with emphasis on activity in inorganic molten salt hydrates. ACS Sustain Chem Eng 1(8):858–870

Sethi S, Ray BC (2015) Environmental effects on fibre reinforced polymeric composites: evolving reasons and remarks on interfacial strength and stability. Adv Colloid Interface Sci 217:43–67

Sgriccia N, Hawley M, Misra M (2008) Characterization of natural fiber surfaces and natural fiber composites. Compos Part A Appl Sci Manuf 39(10):1632–1637

Shamsuri A, Abdan K, Kaneko T (2021) A concise review on the physicochemical properties of biopolymer blends prepared in ionic liquids. Molecules 26(1):216

Sundberg A, Sundberg K, Lillandt C, Holmbom BR (1996) Determination of hemicelluloses and pectins in wood and pulp fibres by acid methanolysis and gas chromatography. Nord Pulp Pap Res J 11(4):216–219

Tanasă F, Zănoagă M, Teacă CA, Nechifor M, Shahzad A (2020) Modified hemp fibers intended for fiber-reinforced polymer composites used in structural applications: a review. Polym Compos 41(1):5–31

Victoria A, Ries ME, Hine PJ (2022) Use of interleaved films to enhance the properties of all-cellulose composites. Compos Part A Appl Sci Manuf 160:107062

Walden P (1914) Molecular weights and electrical conductivity of several fused salts. Bull Imp Acad Sci 1800

Wang S, Lu A, Zhang L (2016) Recent advances in regenerated cellulose materials. Prog Polym Sci 53:169–206

Wang Y (2008) Cellulose fiber dissolution in sodium hydroxide solution at low temperature: dissolution kinetics and solubility improvement. PhD thesis, Georgia Institute of Technology

Xu J, Cheng JJ, Sharma-Shivappa RR, Burns JC (2010) Sodium hydroxide pretreatment of switchgrass for ethanol production. Energy Fuels 24(3):2113–2119

Zhang X, Ries ME, Hine PJ (2021) Time-temperature superposition of the dissolution of silk fibers in the ionic liquid 1-ethyl-3-methylimidazolium acetate. Biomacromol 22(3):1091–1101